Time-dependent flexural behaviour of prestressed alkali-activated concrete (AAC) girder with cast-in-situ AAC topping

Qian, Zhenxu; Zhang, Shizhe; Ye, Guang; Matthys, Stijn; Luković, Mladena

DOI
10.1016/j.conbuildmat.2025.141615

Publication date
2025

Document Version
Final published version

Published in
Construction and Building Materials

Citation (APA)
Qian, Z., Zhang, S., Ye, G., Matthys, S., & Luković, M. (2025). Time-dependent flexural behaviour of prestressed alkali-activated concrete (AAC) girder with cast-in-situ AAC topping. *Construction and Building Materials*, *484*, Article 141615. https://doi.org/10.1016/j.conbuildmat.2025.141615

Construction and Building Materials 484 (2025) 141615

Contents lists available at ScienceDirect

Construction and Building Materials

journal homepage: www.elsevier.com/locate/conbuildmat

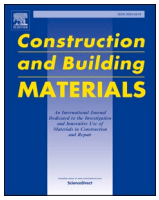

Time-dependent flexural behaviour of prestressed alkali-activated concrete (AAC) girder with cast-in-situ AAC topping

Zhenxu Qian [a,*], Shizhe Zhang [a], Guang Ye [a,b], Stijn Matthys [b], Mladena Luković [a]

[a] Faculty of Civil Engineering and Geosciences, Delft University of Technology, Delft, the Netherlands
[b] Faculty of Engineering and Architecture, Ghent University, Ghent, Belgium

ARTICLE INFO

Keywords:
Alkali-activated concrete (AAC)
Composite prestressed girder
Time-dependent flexural behaviour
Prestress loss

ABSTRACT

Alkali-Activated Concrete (AAC) is considered as a promising alternative to conventional Portland Cement Concrete (PCC) due to its potential to reduce environmental impacts. However, its application in practical engineering is limited by, among others, insufficient understanding of the long-term structural behaviour of reinforced and prestressed AAC elements. To address this, a series of experiments were conducted on composite girders to investigate the long-term flexural behaviour. The composite girder is formed by a prefabricated prestressed AAC inverted-T girder with cast-in-situ ACC topping concrete. The midspan deflection of two composite girders, subjected to self-weight and additional sustained loading, were measured over a 9-month period. Subsequently, flexural tests under four-point bending configuration were performed at the age of 9 months and the reference age of 28 days. The results showed that the specimens tested at 9 months exhibited reduced initial stiffness, decreased cracking load and larger crack widths in the precast prestressed girder compared to those tested at 28 days. The reduction in stiffness likely stems from decreased elastic modulus and structural cracking. Meanwhile, the lower cracking load arises from prestress losses caused by ongoing (restrained) shrinkage and creep, consistent with AAC material test observations. Larger crack widths observed in the precast girder may result from a degradation of bond between AAC and prestressing strands over time. The distinct failure patterns of the 9-month specimens (anchorage failure for sample subjected to self-weight only and flexural failure for sample exposed to additional sustained load), highlighted the role of creep on bond behaviour between prestressing strands and AAC, particularly as a function of varying stress levels at the level of strands. Finally, analytical models were applied to evaluate the prestress loss and flexural behaviour of the specimens. The effective prestressing force and cracking loads at both testing ages were overestimated when the effects of (partially) restrained deformations between precast and cast-in-situ AAC were neglected. More accurate analytical predictions were achieved when these long-term effects and the level of restraint in the composite girder were considered.

1. Introduction

Concrete is the most widely used construction material in the world, primarily due to its good functional performance, broad availability and low cost [1]. However, the production of Portland Cement (PC), a key ingredient of concrete, is one of the largest contributors to global CO_2 emissions, accounting for up to 5–8 % of worldwide CO_2 emissions [2,3]. As a result, efforts have been made to mitigate the carbon footprint by developing environmentally friendly alternatives to conventional PC-based concrete (PCC). Among those alternatives, Alkali-Activated Concrete (AAC), based on the chemical reaction between alkali activators and industrial by-products, has gained significant attention [4,5]. In addition to the reduced environmental impact and utilization of industrial waste, some AAC mixtures show material properties comparable to, or even superior to, those of PCC [6]. However, the application of AAC remains limited due to the knowledge gap between its material properties and structural performance. These limitations arise from the challenges in generalizing the behaviour of AAC, which encompasses a wide range of materials, each with varying precursors and activators.

To enable the safe structural application of AAC, research has

* Corresponding author.
E-mail addresses: Z.Qian-2@tudelft.nl (Z. Qian), Shizhe.Zhang@tudelft.nl (S. Zhang), G.Ye@tudelft.nl (G. Ye), Stijn.Matthys@UGent.be (S. Matthys), M.Lukovic@tudelft.nl (M. Luković).

https://doi.org/10.1016/j.conbuildmat.2025.141615
Received 30 December 2024; Received in revised form 17 April 2025; Accepted 1 May 2025
Available online 21 May 2025

increasingly focused on the structural behaviour, but mostly limited to short-term studies, typically up to 28 days of curing. Several studies have concluded that AAC demonstrates higher bond strength with steel compared to PCC owing to relatively higher tensile strength of AAC [7]. Furthermore, reinforced AAC and PCC members tested at 28 days have been found to exhibit similar load-bearing capacity and cracking behaviour [8–12]. Several researchers have suggested that the analytical models developed for PCC members can conservatively predict the short-term bond strength and ultimate load-carrying capacity of AAC structural elements [7,13]. Contradicting trends were also reported [14]. Furthermore, only few studies have investigated prestressed AAC beams [15,16], focusing primarily on their short-term flexural behaviour.

Analytical models developed for conventional concrete are reported to conservatively predict the short-term behaviour of AAC members [7]. Still, their validity for long-term behaviour, which is crucial for structural design, remains unclear. Moreover, unlike PCC, which often gains strength beyond 28 days, certain types of AACs have shown notable reductions in key material properties, including compressive strength, tensile strength, flexural strength, and elastic modulus [11,17,18]. These reductions may be attributed to various mechanisms, depending on the specific mixture composition, such as carbonation, drying shrinkage, microcracks and chemical changes in microstructure due to drying [18]. In addition, some AAC mixtures exhibit higher shrinkage and creep compared to PCC [19–22]. Understanding the influence of aforementioned time-dependent material properties and the coupled hygro-chemo-mechanical effects on the long-term performance of AAC members, particularly prestressed elements, is critical. However, only two studies have examined the long-term behaviour of reinforced AAC. Flexural tests on reinforced beams produced by two types of AAC (GGBFS-based AAC and FA-based AAC) were carried out up to 151 days, and the reductions in cracking load, bending stiffness and tension stiffening effects, as well as increased crack width, were reported over time [11,18]. Additionally, Un et.al [23] monitored the long-term deflection of reinforced beams using a specific mixture and validated the feasibility of prediction methods developed for PCC with experimentally obtained material input. It is also concluded that unlike PCC, where the input parameters can be estimated from compressive strength through empirical relationships, the material properties of AAC need to be experimentally measured. Despite these findings, the long-term behaviour of prestressed AAC elements, including prestress losses, remains fully unexplored. Given the potential of prestressed AAC members for large-scale construction, investigating their long-term behaviour is crucial to enable their safe application.

This study investigates the time-dependent flexural behaviour of prestressed AAC girders with cast-in-situ AAC topping, a common construction system in the Netherlands. The research involved a short-term flexural test on a composite girder at 28 days. Additionally, the long-term deflection of two girders subjected to different load levels were monitored for 9 months, followed by tests under flexure performed at 9 months. The development of material properties for the applied AAC mixtures was also measured over time. Finally, the structural performance of the composite girders under flexure was analysed using analytical models. The predicted prestress losses, cracking loads, and ultimate capacity were compared to experimental results. Given the pronounced shrinkage and creep of AAC, accounting for the effects of (restrained) differential deformations in composite girder is necessary for accurate analytical predictions. This investigation provides insights into the time-dependent performance of prestressed AAC structures, encompassing both material and structural aspects.

2. Material and tests

2.1. Material preparation

Two types of AAC were used to fabricate the composite girders. Self-compacting AAC was used for the precast prestressed girders and is referred to as self-compacting geopolymer concrete (SCGC) [24]. A ready-mixed AAC provided by SQAPE B.V, was used for cast-in-situ topping and is referred to as topping AAC. The composition of SCGC is listed in Table 1. Topping AAC consists of 400 kg of aluminosilicate precursor, 180 liters of liquid including alkali activators and 2.5 kg of admixtures per cubic meter.

The material properties of AAC were tested using standard methods developed for PCC. Compressive strength was measured on 150 mm cubes following NEN-EN 12390–3. The elastic modulus was determined on $100 \times 100 \times 400$ mm prisms, according to NEN-EN 12390–13. Splitting tensile tests were conducted on 150 mm cubes as per NEN-EN 12390–6.

After unmoulding at 1 day, SCGC samples were placed in a fog room for moist curing (20°C and RH $>$ 95 %) and subsequently exposed to controlled laboratory conditions (20°C and 55 % RH). One group of samples remained in the fog room until designed testing ages (i.e. up to 190 days for compressive/splitting tensile strength tests and up to 330 days for elastic modulus tests). Three other groups were exposed to drying under controlled laboratory conditions after 7, 14 and 28 days. For topping AAC, compressive strength samples were cured in moist conditions, while prisms were divided into four groups: one group received continuous moist curing, and the remaining three were subjected to moist curing followed by exposure to drying after 7, 14 and 28 days.

The volume stability of SCGC was investigated. Autogenous shrinkage was measured on two samples using an autogenous deformation testing machine (ADTM) until 28 days. The samples were kept sealed. The curing temperature was controlled at 25℃ for 1 day and then kept at 20℃. Detailed information about the ADTM can be found in [25]. Free shrinkage and creep were measured on $100 \times 100 \times 400$ mm prismatic specimens. Free shrinkage was measured at 20℃ and 55 % RH after 7, 14 and 28 days of moist curing according to NEN-EN 12390–16. Creep tests were conducted at 1, 3 days and 28 days, following NEN-EN 12390–17, under a load level of 17 MPa, representing approximately estimated stress level after applying prestress.

FeP1860 prestressing strands were used, with a tensile strength of 1915 MPa and a 0.1 % proof stress of 1694 MPa. The relevant elongation at maximum load and 0.1 % proof stress were 5.95 % and around 1.1 %, respectively. B500B ribbed reinforcement was used for longitudinal reinforcement and stirrups.

2.2. Specimen details and fabrication

The composite girders consisted of a precast prestressed girder and a cast-in-situ topping. The geometry and the layout of prestressing strands and reinforcement of the precast girder and cast-in-situ topping are shown in Fig. 1. The precast prestressed girders were 7350 mm long, with a nominal length of 7000 mm. A total of 16 straight prestressing strands, each with a nominal diameter of 12.9 mm, were arranged in two layers. Among these, 4 prestressing strands were unbonded over 1000 mm from each end. The stirrups were spaced variably over 1350 mm from each end (Fig. 1(c)) and uniformly spaced at 250 mm interval along the remaining 4250 mm of the girder. These precast girders were designed elastically (fully prestressed), using an allowable

Table 1
Mixture composition of SCGC [24].

Materials	Content (kg/m^3)
Blast furnace slag	550.0
NaOH solution (50.0 wt%)	36.9
Sodium silicate solution (48.0 wt%)	80.4
Water	191.5
Retarder	1.375
Sand 0–4 mm	762.2
Gravel 4–16 mm	675.0

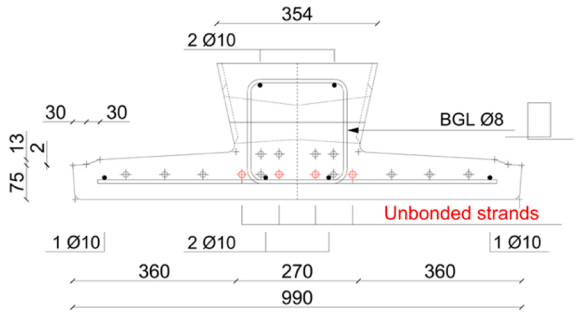

(a) Cross-section and strand layout of precast girder

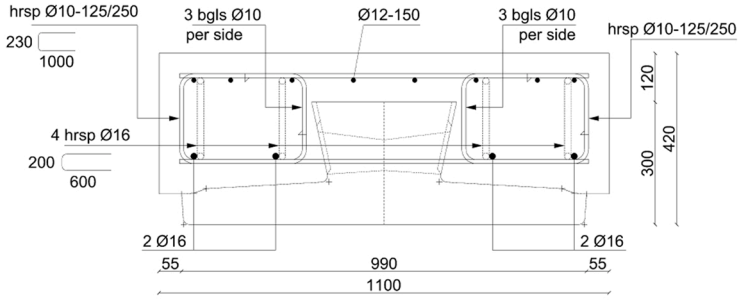

(b) Cross-section and reinforcement layout of cast-in-situ topping

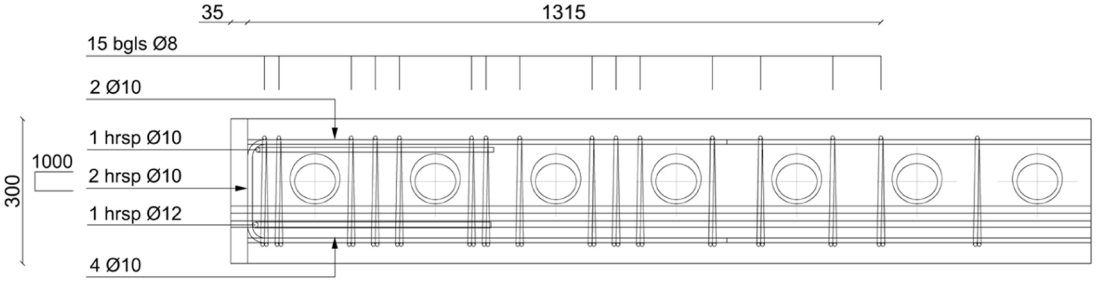

(c) Shear reinforcement layout at the end of precast girder

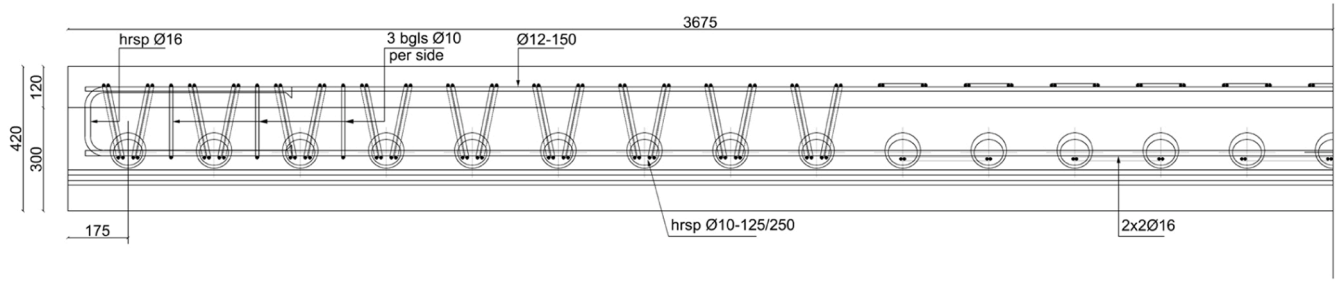

(d) Shear reinforcement layout of cast-in-situ topping

Fig. 1. Geometry and strand/steel layout of precast girder/ cast-in-situ topping (Unit: mm).

stress concept [26]. After casting the girder at the precast factory, prestressing was applied by cutting the strands at 3 days. The girders were then wrapped with moist burlaps and plastic foil for curing. After 31 days, the cast-in-situ topping was cast. The width and total height of the composite section were 1100 mm and 420 mm, respectively.

2.3. Experimental programme

Flexural tests on composite girders were conducted both at short-term (at 28 days) and long-term (at around 9 months). Note that the 9-month monitoring period is described as "long-term", being consistent with the definition in the literature [23,26–28]. The experimental programme is summarized in Table 2.

The composite girder labelled STF was moist cured (covered with burlap and plastic foil) until testing. Flexural test was carried out at 28 days after pouring the topping concrete. The long-term specimens, LTF and LTF_LS, were subjected to more severe curing conditions. They were sealed with plastic sheets for 3 days and then exposed to lab condition (19℃ and 50 % RH) for long-term deflection monitoring. Flexural tests were conducted after approximately 9 months.

Table 2
Experimental programme.

Specimen category	Test method	Testing age*	Specimen preparation	
			Curing condition	Load before testing
Short-Term Flexural (STF)	Flexural test	28 days	Moist cured until testing	Self-weight
	Re-tested under flexure (STF_R2)	240 days	Exposed to lab conditions after 1st round of test	
Long-Term Flexural (LTF)	Flexural test	267 days	Moist cured for 3 days and	Self-weight
Long-Term Flexural under Sustained Load (LTF_LS)	Sustained loading test Flexural test	262 days 274 days	exposed to lab conditions	70 kN for 158 days and 130 kN for 76 days

* Note: the testing age was counted from the date when topping concrete was cast.

2.4. Test setup and measurement

A four-point bending configuration was used for flexural tests at 28 days and 9 months, as well as for the sustained loading tests (Fig. 2(a) and (b)). The load was applied over the full width of the girders through spreader beams. The specimens were supported on a contact area of 350 mm× 280 mm at two ends with hinge and roller supports. The specimen LTF was subjected only to its self-weight, while LTF_LS was exposed to sustained loading after 28 days in two stages: initially under point loads of 70 kN for 158 days, followed by 130 kN for 76 days. The load level of 70 kN corresponded to approximately 65 % of the calculated short-term cracking load, which was subsequently increased to 130 kN, representing the serviceability bending moment calculated according to Load Model 1 [29]. Long-term deformation monitoring started 3 days after casting of the topping concrete.

The flexural tests at 28 days and 9 months were conducted in two phases. In the first phase, the testing protocol included loading/unloading cycles at predefined load levels for monitoring purposes. Load control was applied with a speed of 10 kN/min, which was increased to 20 kN/min for the final load cycles in the long-term flexural tests. In the second phase, when significant non-linear deformations were observed, displacement control was applied.

2D Digital Image Correlation (DIC) was utilized during the flexural tests to monitor crack development in the constant moment zone of the specimens, capturing images from both the side and bottom surfaces of the girder (Fig. 3(a) and (b)), respectively. Additionally, Linear Variable Displacement Transducers (LVDTs) were placed at the soffit of specimens to measure deflection at the midspan.

3. Test results and discussion

3.1. Material properties

Fig. 4(a) displays the development of compressive strength of both SCGC and topping AAC. Under moist curing condition, both materials exhibited an increase in compressive strength over time. The compressive strength of SCGC was not significantly influenced by curing conditions after 3 months, remaining stable or showing a slight increase at later curing age. This trend is consistent with previous studies [11,18] where the GGBFS-based AAC mixture, S100, illustrated an increase in compressive strength up to 91 days and maintained similar strength between 6 months and 5 years.

The development of splitting tensile strength of SCGC is shown in Fig. 4(b). After initial strength development till 7 days, samples under moist curing showed a slight strength increase over time. When samples were exposed to drying, an additional increase in strength after exposure was recorded. The splitting tensile strength of samples exposed to drying after 7 days increased by 30 % between 7 days and 28 days while samples exposed to drying after 28 days saw a 33.2 % increase between 28 days and 91 days. This increase was more pronounced compared to that in compressive strength. However, a slight decrease in splitting tensile strength followed. At 6 months, the splitting tensile strength of the samples exposed to drying after 7 days, 14 days and 28 days decreased by 10.5 %, 5.9 % and 11.9 %, respectively, compared to their peak strength. This apparent strength increase and subsequent decrease can be partially attributed to eigenstresses caused by hygral gradients during drying, as explained in [30]. However, part of this reduction is permanent and due to microstructural changes of AAC [18].The development of splitting tensile strength of GGBFS-based AAC (S100) was published in a previous study [18].The tests were conducted on the 100 mm cubes exposed to drying after 28 days. Different from SCGC samples (150 mm cubes), S100 samples show a 12 % drop in splitting tensile strength between 74 days and 91 days, which might be attributed to the shorter duration of eigenstresses (as hygral equilibrium is reached faster) in smaller samples [30].

The evolution of the elastic modulus for both SCGC and topping AAC is plotted in Fig. 4(c). Under standard curing, the elastic modulus of SCGC reached a plateau after 14 days, while topping concrete continued to increase slightly until 81 days. However, upon exposure to drying, the elastic modulus of both SCGC and topping AAC started to decrease. Even after 28 days of moist curing followed by drying, SCGC specimens showed a 32 % reduction in elastic modulus between 28 and 330 days. Meanwhile topping AAC saw an 8.3 % decline between 30 and 81 days. Similar reduction in the elastic modulus of AAC has been reported in previous studies [18,31]. The chemical change in the microstructure under drying condition were reported to induce microcracking of GGBFS-based AAC [18]. Additionally, carbonation might have contributed to this phenomenon. SCGC showed higher carbonation depth compared to S100 in [18]: with approximately 3 mm and 7.5 mm after 3 months and 9 months, respectively. Nedeljković et al. [32] reported a significant decline in elastic modulus measured in carbonated GGBFS/FA-based AAC paste by nano-indentation. The combined effects of drying and carbonation likely contributed to the reduced mechanical properties of SCGC. Since the drying environment of 55 % RH falls within the optimal range for carbonation (50 %-80 %) [33], drying-induced cracks might provide pathways for CO_2, further accelerating carbonation.

Fig. 5(a) presents the autogenous shrinkage and free shrinkage of SCGC. Autogenous shrinkage developed rapidly at an early age, reaching about 650 μm/m by 3 days, which accounts for approximately half of the value measured at 28 days. Free shrinkage after 2.7 years was 1156 μm/m, 1005 μm/m and 775 μm/m for SCGC samples exposed to drying after 7, 14 and 28 days of moist curing, respectively (see Fig. 5(b)). This indicates that prolonged moist curing helps to reduce free shrinkage. However, a continuous increase in free shrinkage was observed for all specimens over the 2.7 years period.

(a) Short-term and long-term flexural tests (b) Sustained loading test (LTF and LTF_LS)

Fig. 2. Test configuration of flexural tests on composite girders.

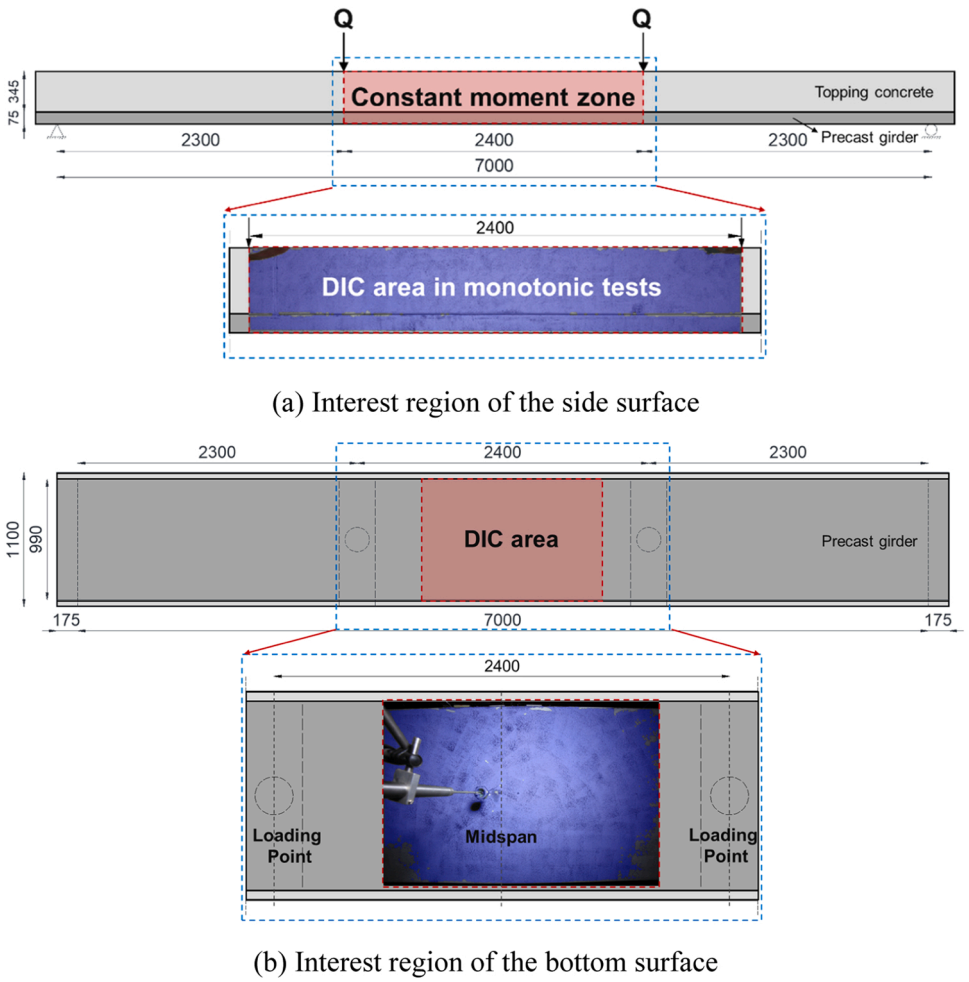

Fig. 3. Test setup of the flexural test with indicated area for Digital Image Correlation (DIC) analysis (Dark grey represents region of precast girder and light grey represents region of topping concrete; Unit: mm).

The creep deformation of SCGC, loaded at a stress level of 17 MPa at 1, 3 and 28 days are shown in Fig. 5(c). When loaded at 1 day, creep deformation reached around 2200 μm/m by 80 days. When loaded later, at 3 and 28 days, the deformation reached 1700 μm/m and 1150 μm/m, respectively.

Compared to conventional concrete with a similar strength class, SCGC showed considerably higher autogenous shrinkage, free shrinkage and creep [21]. The continuous increase in shrinkage and creep may result in a long-term reduction of prestress force. To mitigate prestress losses caused by autogenous shrinkage and creep, prestressing was introduced at 3 days, rather than at 1 day, which is more typical for the fabrication of PCC prestressed girders in the Netherlands. In addition, the specimens were covered with moist burlaps and plastic sheets in the initial stage to avoid moisture loss.

3.2. Structural behaviour

3.2.1. Time-dependent deformation under sustained loading and self-weight

The long-term midspan deflection of specimen LTF and LTF_LS is plotted in Fig. 6. Negative values indicate hogging (upward deflection), while positive values indicate sagging. Initially, both specimens were subjected to the same loading/boundary conditions, resulting in similar deflections. The bottom fibre of the girders was under compression due to prestressing, counteracting the tension induced by their self-weight. Combined with creep effects, this led to continuous hogging of LTF, reaching 8.8 mm over 9 months. A similar trend was observed in pre-stressed monolithic beams made of conventional concrete subject to sustained loading for five years [26], where midspan deflection continuously increased over time. This behaviour could not be represented by a time-dependent function proportional to the creep function, which is generally used to describe the time-dependent development of camber for uncracked beams. The phenomenon was attributed to the presence of non-prestressed steel and a redistribution of stress between steel and concrete [26]. Note that, the maximum stress level in [26] was around 42 % of its mean prism compressive strength at the moment of prestressing, whereas it was around 50 % in the presented research. To control camber, it was advised to choose the level of prestressing as a function of the permanent load [26], in order to avoid excessive deformations and reduce creep effects.

The deflection of LTF_LS reached a plateau shortly after applying the load of 70 kN, remaining nearly constant over the following 6 months. No flexural cracks were observed at the bottom of LTF_LS during this stage. At 186 days, when further loading to 130 kN (corresponding to SLS moment in the bridge), the deflection first instantly increased to 8 mm due to elastic deformation and then gradually increased to 10.6 mm over the next 3 months. After unloading, partial recovery of the midspan deflection was observed, with values of 9.5 mm, 10.5 mm and 11.1 mm after 2 hours, 2 days and 4 days, respectively. The residual deflection after unloading suggests a slight reduction in stiffness.

As shown in Fig. 7(a), a horizontal crack was observed between precast girder and topping concrete in both LTF and LTF_LS, starting from the edge of the specimens. Drying cracks were also found on the topping concrete of both specimens (see Fig. 7(b)). Delamination and cracking are due to the (restrained) differential deformations between

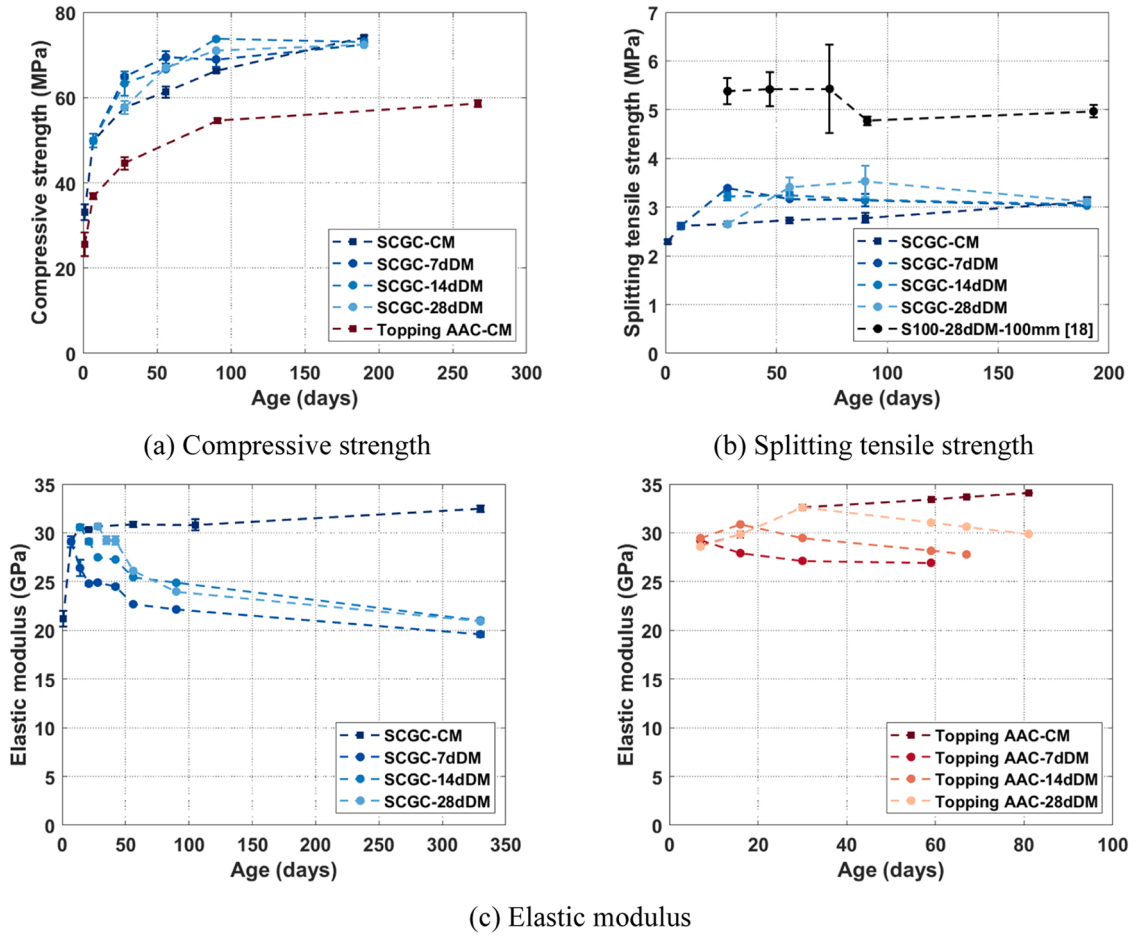

Fig. 4. Development of mechanical properties: CM- continuous moist curing; DM- moist curing and subsequently exposed to drying.

precast and topping AAC. Both specimens for long-term monitoring underwent harsh curing, as they were exposed to lab condition after only 3 days of sealed curing. This likely contributed to drying cracks and delamination. During the second loading stage at 130 kN, minor cracks were observed at the soffit of LTF_LS in the constant bending moment region. The cracked/delaminated section led to a reduction in flexural stiffness, resulting in an increase in midspan deflection. The long-term deflection observed in the loaded girders (during loading stage of 130 kN) is consistent with the behaviour of a partially prestressed beam reported in [26].

3.2.2. *Flexural behaviour of short-term and long-term specimens*

Fig. 8 shows the load-deflection relationship for the short-term (STF) and long-term flexural tests (LTF and LTF_LS) as well as the re-test on STF (STF_R2). The load is defined as the average of point loads applied to the girder. It should be noted that different loading schemes were applied: LTF and LTF_LS were subjected to loading/unloading cycles (see Fig. 8(a)). Given the significant nonlinearity observed after applying cycles with high load levels, the focus of the comparison among the three girders is on their load-deflection behaviour and cracking patterns before 190 kN (Fig. 8(b), right).

There is a significant stiffness reduction in the girder tested at 9 months compared to that tested at 28 days: STF specimen had the highest stiffness, followed by the stiffness of LTF_LS and LTF. The load levels when reaching the turning point from elastic to inelastic stage for specimen LTF and LTF_LS were around 130 kN and 150 kN, respectively, while it was around 190 kN for STF. This is due to reduction of mechanical properties and structural cracking. Elastic modulus of the applied AAC exposed to lab condition is found to decrease over time, which reduces the overall stiffness of the girders. Besides, the delamination and cracking observed during the sustained loading tests likely contribute to the reduction in flexural stiffness of the long-term specimens.

To better track the crack propagation on precast girder and topping concrete, DIC measurement was applied on the bottom and side surfaces of the samples. Crack pattern on the bottom surface of three samples is depicted in Fig. 9. Cracks were first observed on the bottom surface of the precast girders. A minor crack initiated close to the midspan of STF at 90 kN, which was significantly earlier than the observed stiffness change (around 190 kN). From the crack pattern of STF (Fig. 9(a)), it can be observed that at 190 kN, this crack propagated throughout the whole width of the girder. This likely caused the stiffness reduction observed in the load-deflection response. Compared to STF tested at 28 days, the cracking load for LTF tested at 9 months was 44 % lower, due to prestress loss over time. Shrinkage and creep of SCGC, continuously increased within the testing period of 9 months. LTF possibly exhibited more severe shrinkage as it was exposed to lab condition at 3 days after casting topping concrete. Among the three specimens, LTF_LS had the lowest cracking load at 40 kN. Minor cracks initiated under the sustained load and reopened during the flexural test.

Unlike STF which showed only minor cracks, LTF exhibited severe cracking throughout the section at serviceability load level of 130 kN, resulting in the degradation of overall stiffness of the specimen. At this load level, multiple cracks could be observed on LTF_LS. These cracks further extended across the width of the girder at 160 kN, leading to the stiffness reduction. At 250 kN, spacings between major cracks were similar in all samples. Still, multiple cracks with smaller crack widths were captured in STF, which were not observed in 9-month samples. In

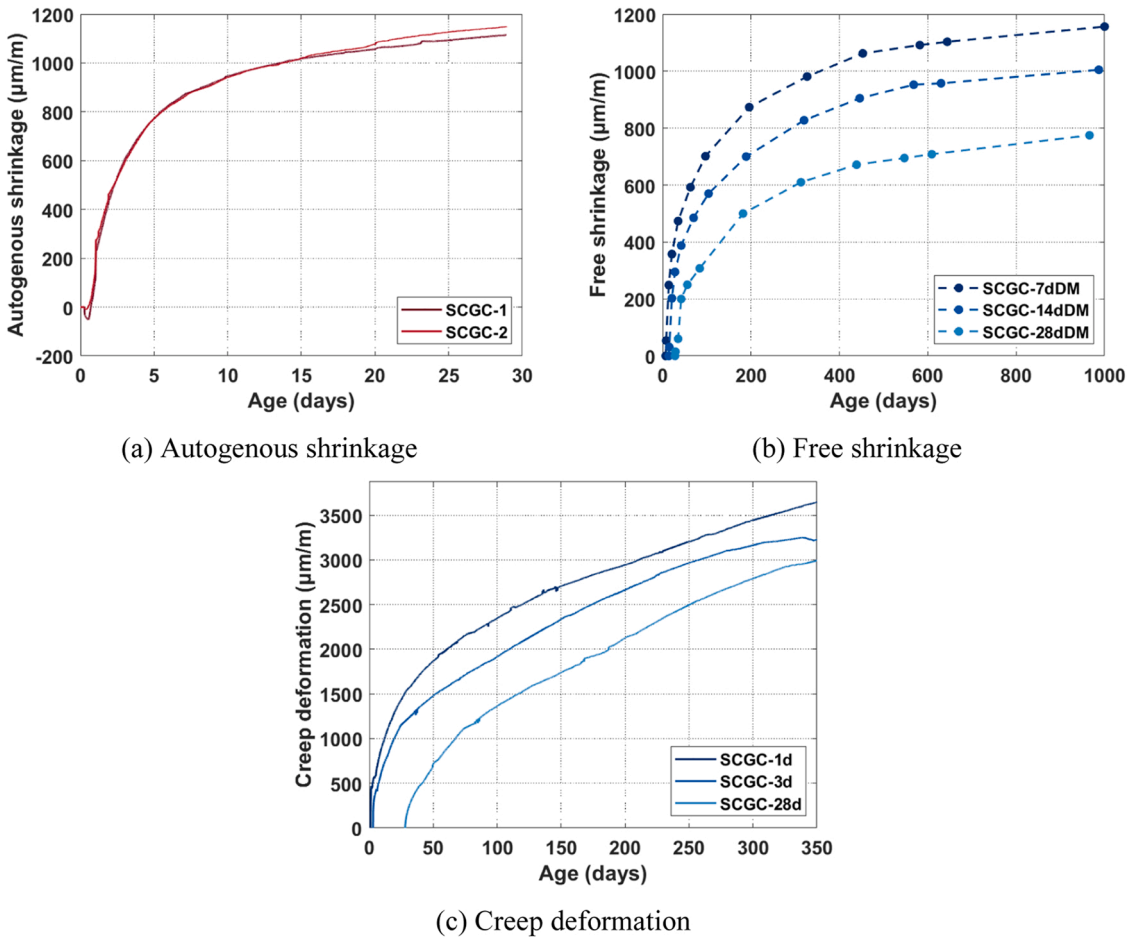

Fig. 5. Volume stability of SCGC: DM- moist curing and subsequently exposed to drying.

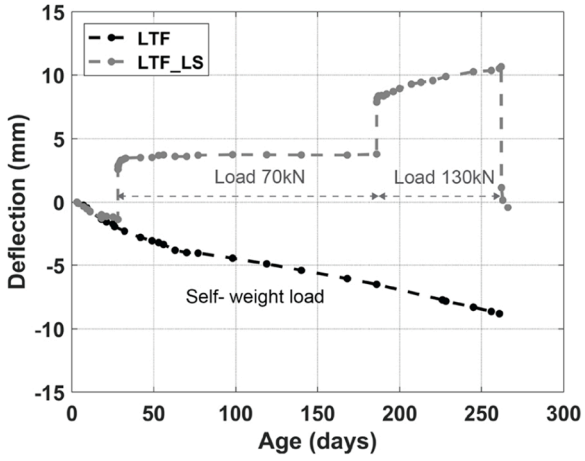

Fig. 6. Long-term deflection of the girders subjected to self-weight, LTF and, to self-weight and sustained load, LTF_LS. Deflection was monitored starting 3 days after casting of the topping concrete (34 days after casting of the pre-stressed girder).

general, LTF and LTF_LS had fewer cracks with larger crack widths compared to STF, possibly due to the effect of creep on bond behaviour between prestressing steel and concrete. Note that quantification of crack width on the bottom surface of the girders was not feasible due to out-of-plane movement, which affected the accuracy of 2D DIC measurements.

Fig. 10 illustrates the crack pattern on the side surface of the specimens at the indicated load levels. Cracking in all specimens consists of a combination of vertical flexural cracks and a horizontal debonding crack between the precast girder and the topping concrete. Delamination was first observed at approximately 190 kN in all the specimens, initiating near the edge of the constant bending moment region and further extending toward the mid-span. The development of debonding crack led to a gradual loss of composite action between precast girder and topping concrete, and could be considered as one of the main contributors to the reduction in global flexural stiffness of the specimens. Furthermore, due to debonding, cracking behaviour on precast girder versus topping concrete were different. On the precast girder, multiple cracks appeared in LTF at 130 kN, and in LTF_LS at 160 kN, confirming the beneficial influence of permanent load in fully prestressed girders. Sustained load reduced the compressive stresses at the level of prestressing strands, thereby reducing the creep effects. In STF, cracks in the precast girder were observed at 190 kN. Unlike in LTF and LTF_LS, this cracking at the bottom of precast girder was preceded by flexural cracking in the topping concrete (Fig. 10 (a)). Compared to the short-term flexural test at 28 days, the specimens tested at 9 months illustrated fewer cracks with larger cracking spacing on the precast girder at the same load. The total number of cracks recorded in the constant moment region of the precast girders, just before failure were 17 and 14 for STF and LTF, respectively. Similar observations can be found on the bottom surface (see Fig. 9). Regarding topping concrete, LTF also exhibited fewer cracks compared to STF, which might be attributed to the debonding crack.

Fig. 11 presents the crack width-load response of the girders. For LTF and LTF_LS girders, only crack widths until 190 kN were considered, as

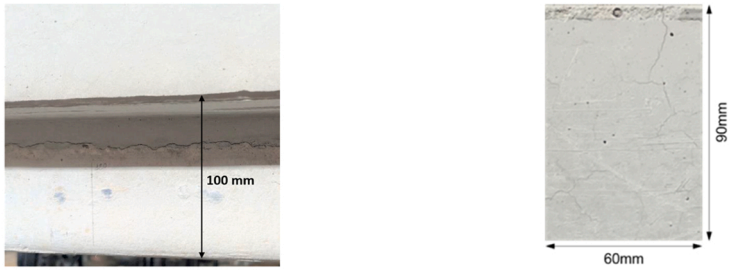

(a) Debonding crack between precast and cast-in situ AAC (b) Drying cracks cast-in situ topping (side view)

Fig. 7. Cracks observed on LTF and LTF_LS during the period of long-term monitoring of deformation.

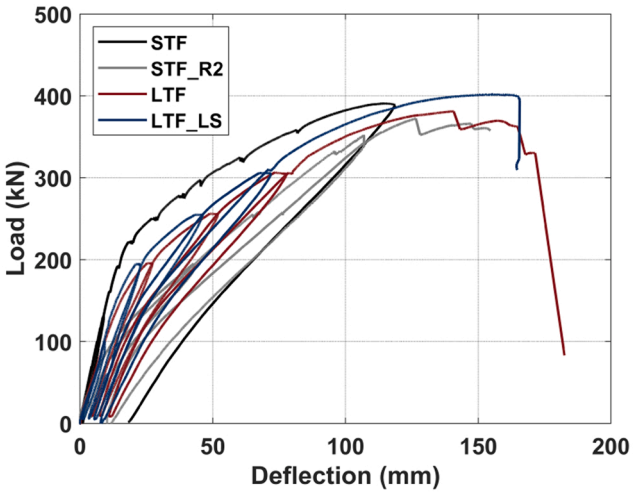

(a) Load-deflection curve with loading cycles

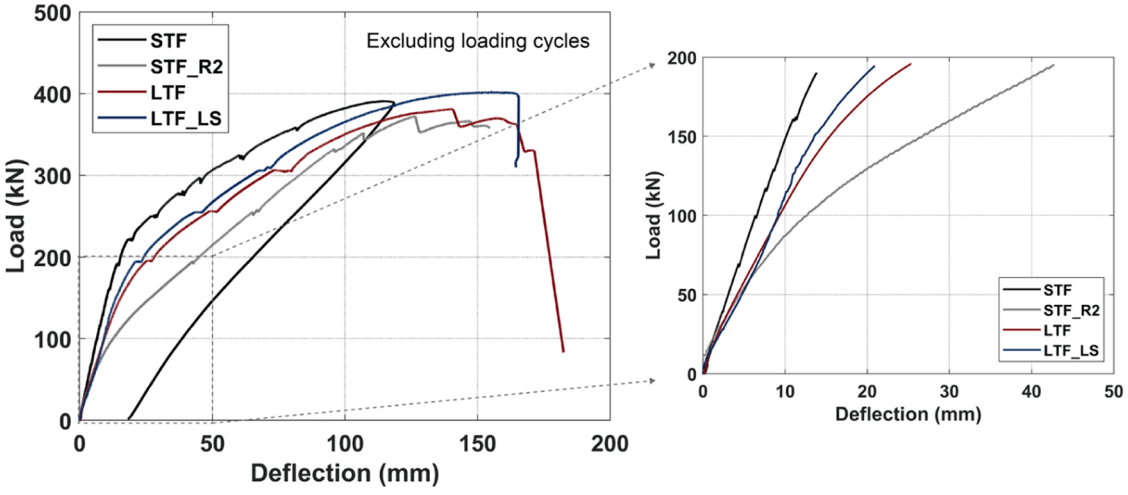

(b) Load-deflection curve excluding loading cycles

Fig. 8. Load-deflection relationship of all samples (load refers to average of point loads).

unloading-reloading cycles were applied at higher load levels. In the precast girder of STF, the crack width criterion of 0.2 mm [34] was reached at the load level of 220 kN. This load is significantly higher than the acting SLS load for a single girder (~130 kN). In contrast, the maximum crack width in the precast girder specimens tested at 9 months reached the limit of 0.2 mm at 160 kN for LTF and 180 kN for LTF_LS. When comparing crack widths at the same load level, the smallest crack width was measured on the specimen tested at 28 days. Specimen LTF showed larger cracks compared to LTF_LS.

The global cracking behaviour of the composite girder was affected by combined effects, including bond between prestressing strands/reinforcement and AAC, bond between precast girder and topping

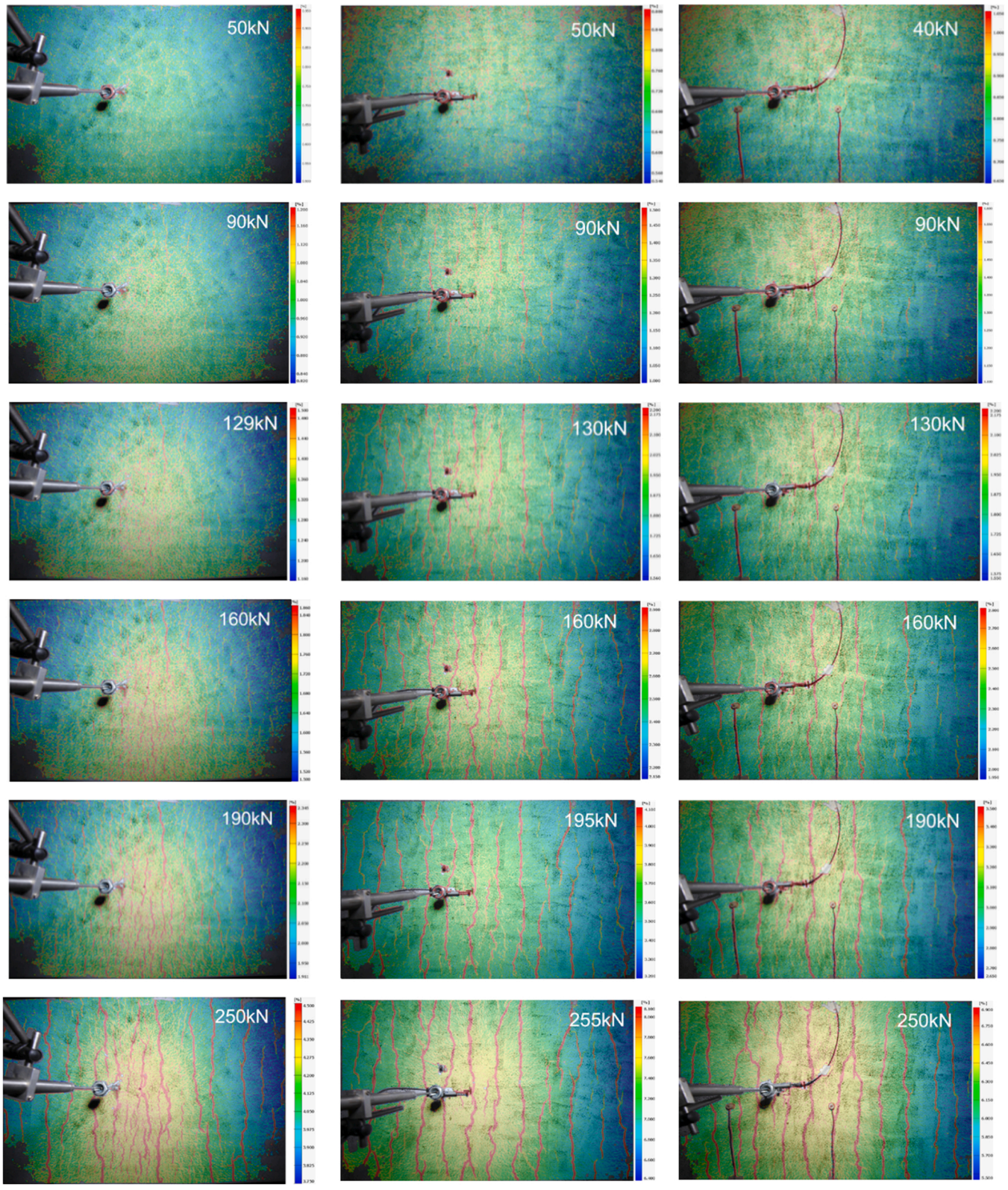

Fig. 9. Crack propagation on the bottom surface of (a) STF tested at 28 days and (b) LTF and (c) LTF_LS, both tested after around 9 months.

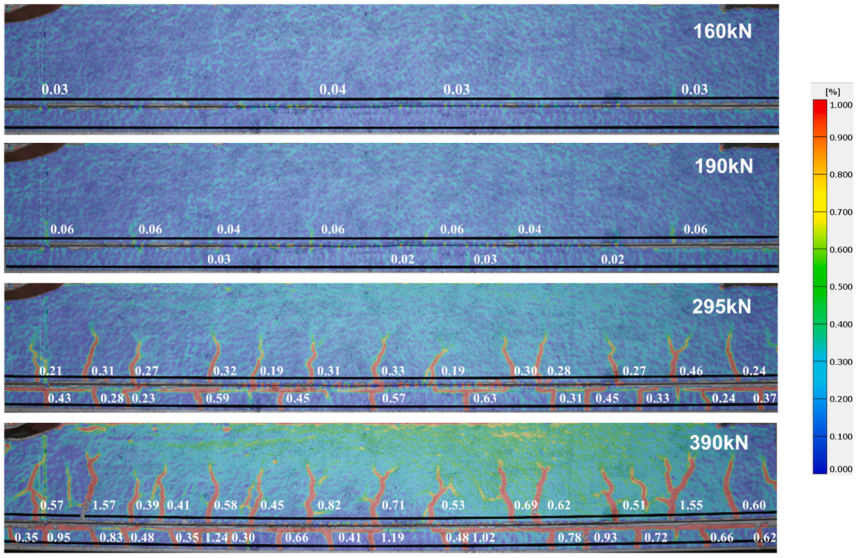

(a) STF

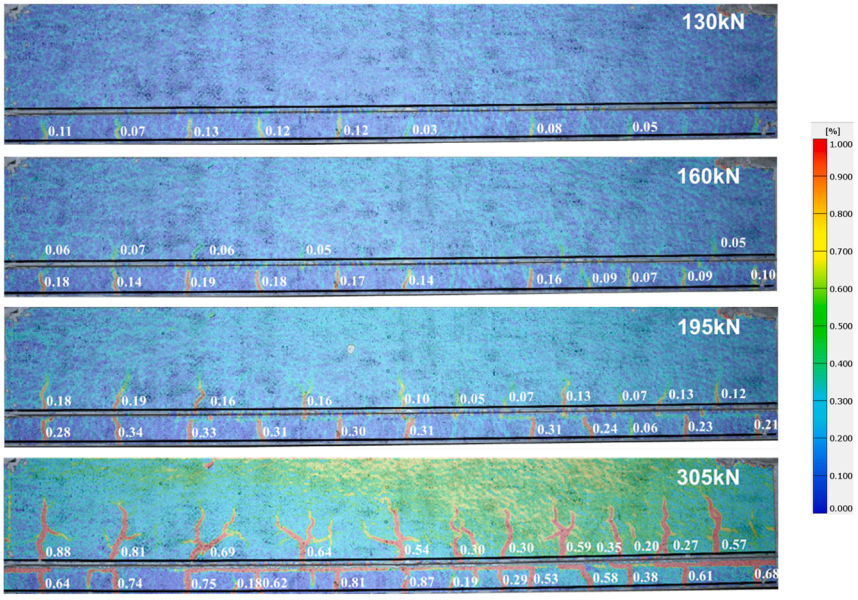

(b) LTF

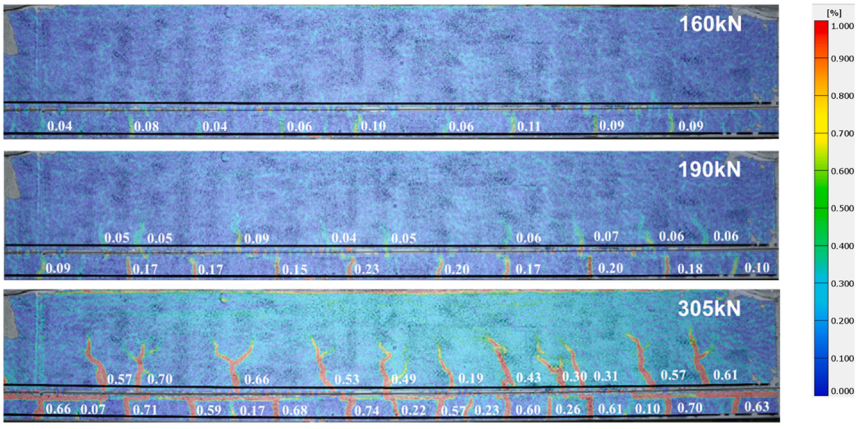

(c) LTF_LS

Fig. 10. Crack pattern on the side surface of STS, LTF and LTF_LS at representative load levels.

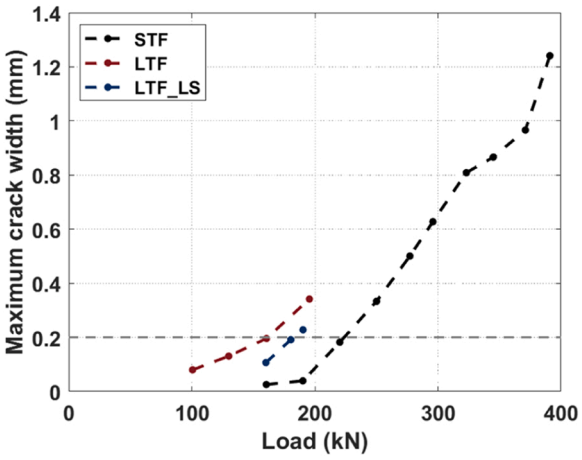

Fig. 11. Maximum crack width-load response on the precast girder of three specimens.

concrete, material properties, etc. Still, the increase in crack width and spacing in the precast girder in long-term test (LTF) compared to short-term test (STF) suggests a possible degradation of bond behaviour between the strands and SCGC over time. This deterioration might result from the time-dependent behaviour of SCGC. One of the contributors is creep effect. Given high creep deformation of SCGC and the role of creep on the bond between reinforcement and conventional concrete [35], bond stress distribution might be affected over time. Besides, due to creep, SCGC tended to contract in the longitudinal direction and expand in the radial direction. This radial expansion resulted in a drop of radial stress around the strand and further reduced the bond capacity in the long term. Additionally, LTF_LS showed more cracks with smaller crack spacing in the precast girder than LTF (Fig. 10), indicating less degradation in bond capacity between strands and SCGC. This may be owing to sustained load, which results in a lower stress level and therefore reduced creep effects in LTF_LS compared to LTF.

The girders exhibited different failure behaviour and load-bearing capacity. In the short-term flexural test, STF reached a maximum load of 390.9 kN with a maximum midspan deflection of 119 mm. The measured strain at the height of prestressing strands was 4.1 mm/m. Considering that the prestressing strand reaches 0.1 % proof stress at about 10 mm/m, and a prestressing strain of around 6 mm/m, the expected yield strain is around 4 mm/m. Although this strain level was close to the measured strain, the specimen did not fail, as the maximum stroke of the jack was reached first. Therefore, this specimen was retested along with LTF and LTF_LS. Fig. 12 (a), (b) and (c) illustrate the failure modes of STF_R2, LTF and LTF_LS, respectively. In LTF, anchorage failure occurred at the load level lower than the maximum load recorded at the 28-day test. A sudden drop of load was recorded at 380.9 kN because of significant strand slippage. Subsequently, the load increased again until the final anchorage failure of the specimen. The flexural crack under the loading point further inclined and led to local crushing of concrete. Similar behaviour was observed for the retested sample (STF_R2), which failed at 372.3 kN, a lower load than the peak load of STF (390.9 kN). This is likely due to the combined effect of load cycles with high load levels and long-term degradation of material properties. On the contrary, LTF_LS exhibited gradual concrete crushing under the loading point, followed by the development of a nearly flat crack in the topping concrete (Fig. 12 (c)), indicating flexural failure at 401.8 kN. Strand slippage was less significant compared to LTF. The different failure modes of LTF and LTF_LS might be attributed to different bond capacities between SCGC and strands. The Hoyer effect, a major contributor to bond stress, changes over time because of the time-dependent properties of concrete [36]. With lower creep effects, the relaxation of Hoyer effect is less pronounced and a lower reduction of bond capacities is achieved. Applying sustained load has a beneficial influence as it reduces the compressive stress at the strand level. This is also reflected in the crack pattern of LTF_LS: more cracks with smaller cracking spacing were observed compared to LTF.

All specimens exhibited significant debonding between the precast girder and the topping concrete. Note that the horizontal passive reinforcement connecting the topping concrete through openings in the web of the prestressed girder (Fig. 1) guarantees continued force transfer after horizontal debonding cracking takes place.

Relying solely on 28-day tests for evaluating the structural resistance of AAC members, as is done with conventional concrete, may lead to inaccurate predictions. Long-term testing at both material and structural levels is crucial for ensuring reliable structural design of AAC components.

4. Analytical analysis of flexural behaviour

4.1. Prestress losses and cracking load

4.1.1. Calculation based on provisions and monitoring measurement

The structural performance of the composite AAC girders subjected to flexure was analysed using analytical models described in EN 1992–1–1 [34]. Given the complexity induced by (varying) sustained load, this analysis focused only on STF and LTF. Prestress losses at 28 days and 9 months (59 days and 298 days after casting the precast girders) were estimated based on the material properties reported in Section 2. The cracking load was further derived and compared to experimental results.

The elastic modulus of SCGC used in the analysis are 25 GPa at 3 days and 27.5 GPa at 31 days. The used volume stability properties of SCGC are summarized in Table 3. The estimated prestress losses (including elastic losses, shrinkage, creep losses and relaxation losses) are 459 MPa for STF and 653 MPa for LTF. The remaining prestress stresses correspond to 67 % and 53 % of the initial prestressing stress applied on the strands (1400 MPa) for STF and LTF, respectively.

Prestress losses were also predicted by using the data obtained from Fibre Bragg Grating (FBG) sensors. The influence of geometry of the girders and thus size effects of drying shrinkage, as well as the change in stress level due to casting of topping AAC and prestress losses can be captured by these sensors. Therefore, the time-dependent deformation at the level of the prestressing strands in composite girders was directly measured [37]. The strain measured by FBG is shown in Fig. 13 (a), reflecting the free deformation of the precast girder (i.e. within first 31 days), and the response of composite girders (i.e. after the topping concrete was cast). However, FBG measurements were available only up to 94 days. To estimate long-term deformation, a predictive model was developed using material test data and validated against FBG measurements. This model was based on principle of superposition proposed by Bažant [38] and used creep compliances measured at 3 and 28 days, along with the adjustment for size effect of drying shrinkage [38]. In the initial stage, when only precast girder was present, a mean stress level of 16.3 MPa was estimated based on linear elastic calculations. After casting topping concrete, the stress level was estimated to reduce to 11 MPa, reflecting the impact of self-weight load of cast-in-situ topping and prestress losses. Considering further the size effect of drying shrinkage (i.e. using a cross-sectional thickness D of 300 mm corresponding to the height of precast girder), the predicted value is close to FBG data (Fig. 13 (b)). The long-term strain development at the level of prestressing strands can further be estimated. The measured strain, including the elastic deformation, shrinkage and creep at 28 days after casting topping concrete is around 2000 μm/m and the predicted strain at 9 months is around 3300 μm/m. Assuming relaxation losses at 28 and 9 months are 10 MPa and 15 MPa, the total prestress losses are calculated to be 410 MPa and 675 MPa, respectively. The remaining stresses correspond to 71 % and 52 % of initial prestressing stress.

The cracking moment of the composite girders is then calculated

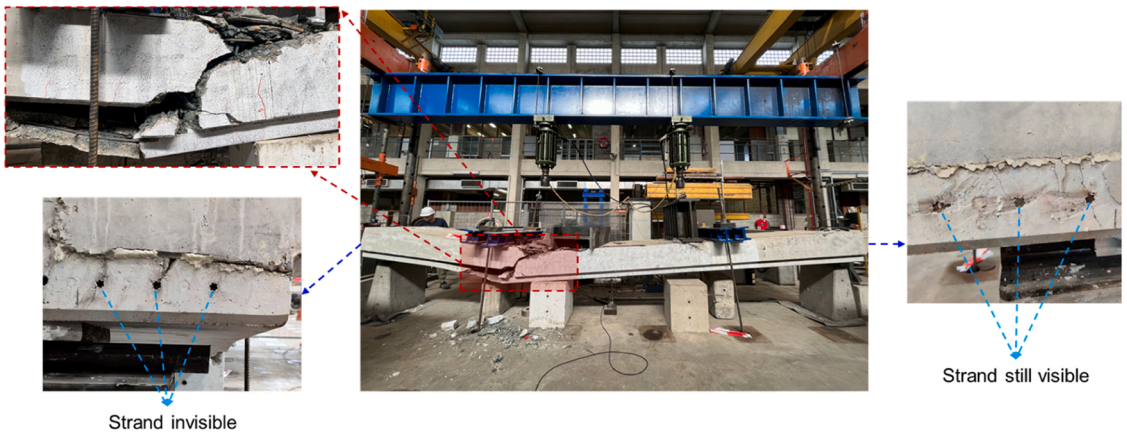

(a) STF_R2: Anchorage failure

(b) LTF: Anchorage failure

(c) LTF_LS: Flexural failure

Fig. 12. Failure modes of (a) STF_R2, (b) LTF and (c) LTF_LS.

based on the remaining prestressing force. Flexural tensile strength of SCGC, estimated from the splitting tensile strength, is used to predict the cracking load. Fig. 14 gives the relationship between the cracking load of the girder and the remaining prestress ratio. The experimental results and analytical prediction at 28 days and 9 months after casting topping concrete are marked in the figure. The remaining prestress ratio in the experiments are estimated from the measured cracking load when the first crack was observed on the bottom surface of the specimens. The weight of spreader beam is considered in calculations.

As shown in Fig. 14, the predicted cracking loads based on the material tests and FBG measurement at 28 days are significantly overestimated compared to experimental results. A similar trend is observed for the 9-month test, where predictions also overestimate the cracking load. In these calculations, the interaction between precast girder and

Table 3
Summary of volume stability properties of SCGC.

Age (days) After casting precast girder	Total shrinkage (μm/m)	Creep (μm/m)	Creep coefficient
31	728	1234	1.9
59	864	1565	2.4
298	1246	3157	4.8

topping concrete is neglected and the girders are assumed to deform freely. This might lead to an underestimation of prestress loss. The effects of restrained deformation on prestress losses are further discussed.

4.1.2. The influence of restrained deformation

There are two critical mechanisms leading to (possible) additional prestress losses caused by restrained deformation: (1) restrained shrinkage of topping concrete (Fig. 15 (a)) and (2) restrained creep of the precast girder (Fig. 15 (b)).

4.1.2.1. Restrained shrinkage of topping concrete due to the presence of the precast girder. The shrinkage of topping concrete induces additional compressive stress in the precast girder, resulting from the combined effects of axial force and bending moment in the precast girder. This contributes to further prestress loss. The final interaction between two parts of the composite member depends on their stiffness difference and the shrinkage rate of SCGC and topping AAC. Note that the restrained creep effects of topping concrete were not considered given the low compressive stress in the topping concrete.

The comparison between autogenous and total shrinkage of topping AAC and total shrinkage of SCGC after 31 days is plotted in Fig. 16. The free shrinkage of SCGC in the period before casting topping concrete is excluded. The curing conditions of STF and LTF were different. Unlike LTF, STF was covered till testing. Therefore, the differential shrinkage for STF is taken as the difference between total shrinkage of SCGC and autogenous shrinkage of topping AAC (178 μm/m). For LTF, it is considered as the difference between total shrinkage of SCGC and topping AAC (264 μm/m, by extrapolation). The creep coefficient (ϕ) of 2.5 according to [34] is used to calculate the effective elastic modulus of topping AAC.

The stress distribution at the centre of the girder due to differential shrinkage for STF and LTF is illustrated in Fig. 17. The resultant compressive stress at the strand level is 0.4 MPa at 28 days and 0.6 MPa at 9 months. These result in additional prestress losses of 2.8 MPa and 4.1 MPa, respectively. Furthermore, as a sensitivity analysis, different combinations of creep coefficient and differential shrinkage were used to calculate the additional prestress loss (Fig. 18). The additional prestress loss caused by restrained shrinkage of topping concrete is low compared to the initial prestressing stress (1400 MPa), even with large differential shrinkage and small creep coefficient (up to 2 % prestress loss).

4.1.2.2. Restrained creep deformation of the precast girder due to topping concrete. Deformation of the prestressed girder due to ongoing creep is (partially) restrained after topping concrete is cast and starts hardening. Assuming fully restrained deformations, the residual prestress force $F_p(t)$ due to restrained creep deformation can be calculated as:

$$F_p(t) = F_{p0} k_\phi(t) \tag{1}$$

where F_{p0} is initial prestressing force and k_ϕ can be expressed as a function of creep coefficient ϕ: [39,40]

$$k_\phi(t) = e^{-\phi(t)} \tag{2a}$$

$$k_\phi(t) = 1 - \frac{\phi(t)}{1 + \rho\phi(t)} \text{ with } \rho = 0.8 \tag{2b}$$

As shown in Fig. 19, the factors k_ϕ obtained from the method proposed by Brakel [39] and Trost [40], as a function of creep coefficient, are similar.

To simulate conditions in the composite girders, the restraint level is further considered by introducing a factor R:

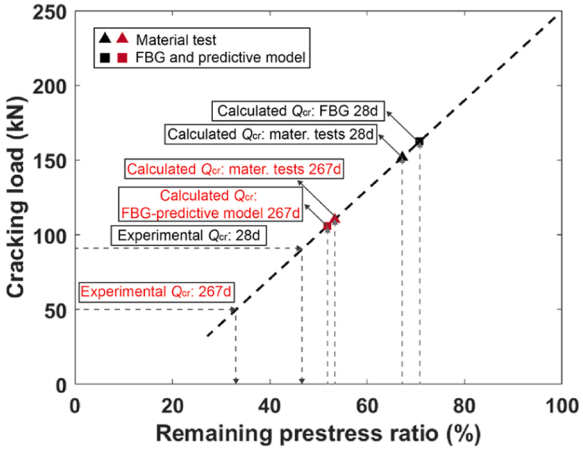

Fig. 14. Prediction of the cracking load depending on prestress loss (28 days and 9 months values are given in black and red, respectively). Note: Calculated Q_{cr} FBG-predictive model 267d refers to the result obtained by aforementioned predictive model (based on material test and verified by FBG measurement).

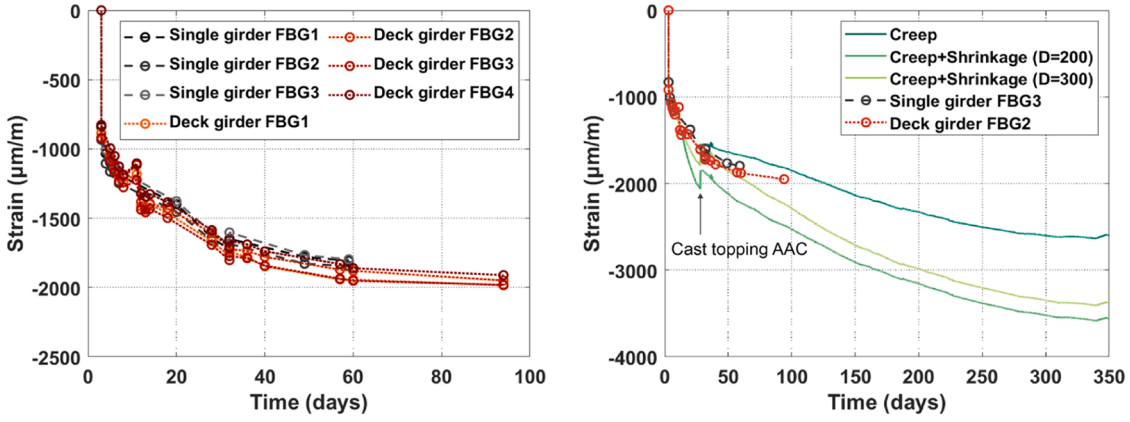

Fig. 13. Time-dependent deformation at strand level (a) FBG data (b) Prediction based on material properties when considering stress level of 11 MPa at strand level after casting topping AAC.

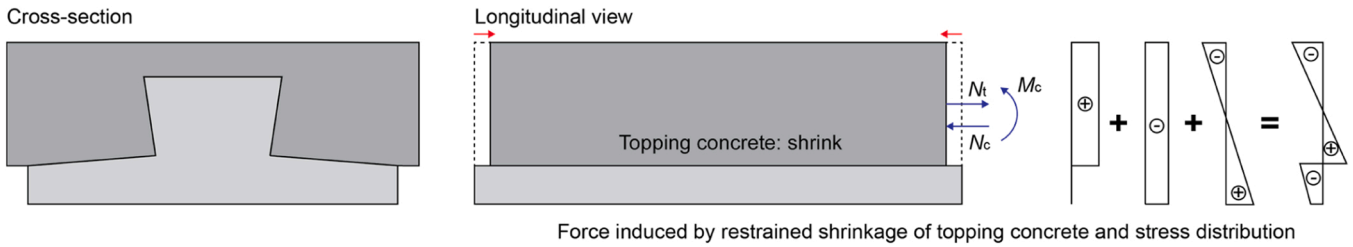

(a) Restrained shrinkage of the topping concrete

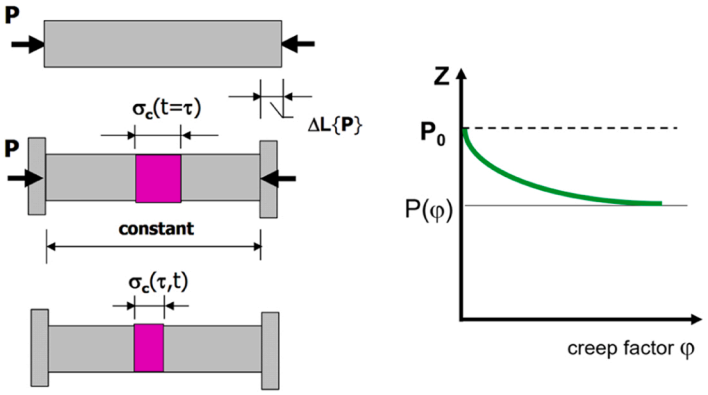

(b) Restrained creep of the precast girder

Fig. 15. Effect of restrained deformations on prestressed losses.

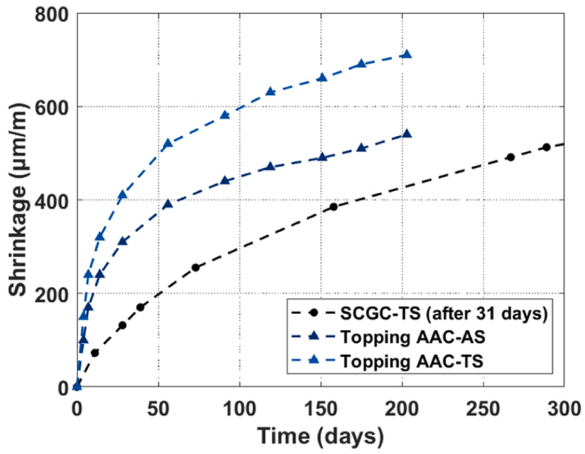

Fig. 16. Differential shrinkage between SCGC and topping AAC: TS- total shrinkage and AS- autogenous shrinkage.

$$R = \frac{A_t/\eta}{A_t/\eta + A_g} \tag{3}$$

where A_t and A_g are the area of topping concrete and precast girder, respectively. η is the ratio between the elastic modulus of SCGC and topping AAC. A modified factor $k_{\phi,R}$ is proposed (Eq. (4)) and the residual prestress force considering the restraint level R can further be calculated following Eq. (5). Note that the modified factor $k_{\phi,R}$ is taken as a constant value for simplification, even though restraint level may change due to ongoing hydration. Besides, the influence of debonding crack observed on LTF during the 9-month monitoring period (Fig. 7(a)) is not considered. This is reasonable as the horizontal reinforcement was applied to connect precast girder and topping concrete. This assumption should be further verified in future.

$$k_{\phi,R}(t) = \left[k_\phi(t) - 1\right]R \tag{4}$$

$$F_{p,R}(t) = F_{p0}k_{\phi,R}(t) \tag{5}$$

The results of creep tests on SCGC sample loaded at 28 days are used to estimate the residual prestressing force. The creep coefficient of

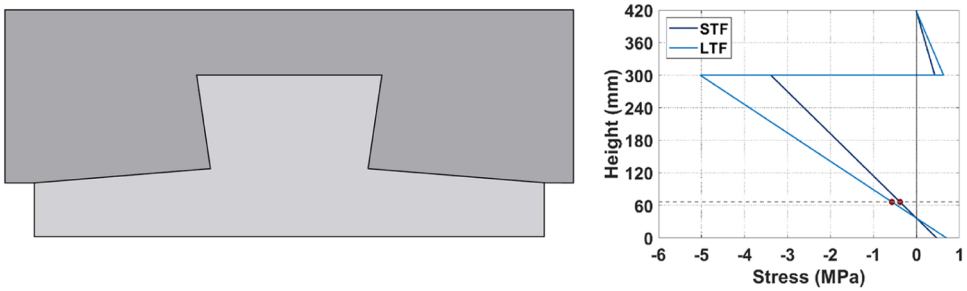

Fig. 17. Stress distribution in the middle of cross-section due to restrained shrinkage on STF and LTF.

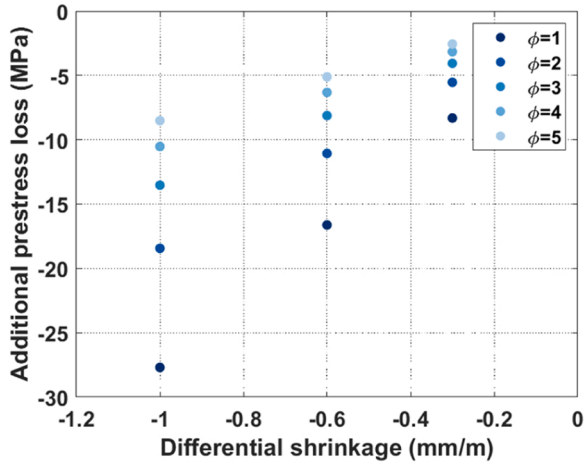

Fig. 18. Parametric study on additional prestress loss as a function of shrinkage and creep coefficient.

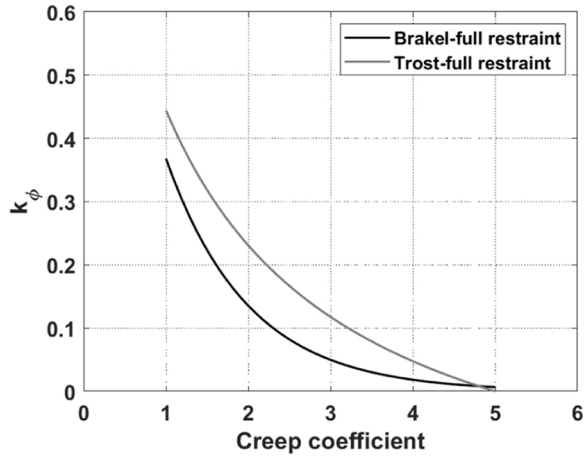

Fig. 19. k_ϕ obtained from the method proposed by Brakel and Trost.

SCGC, when loaded at 28 days, is 1.2 and 4.3 at 28 days and 267 days after loading, corresponding to the time when the flexural tests for STF and LTF were performed. The prestress force at 28 days after casting precast girder (F_{p0}) is assumed to be approximately 76 % of the initial prestress force, based on prestress loss obtained from FBG measurement (1700 μm/m at 28 days, see Fig. 13 (a)). The restraint level due to cast-in-situ topping is calculated as 64 %. A summary of the predicted results obtained from analytical models and tests for STF and LTF are listed in Table 4. The relationship between remaining prestress ratio and creep

Table 4
Summary of predicted results and test results.

	Remaining prestress (%)		Cracking load (kN)		Maximum flexural load (kN)	
Age (days)	28	267	28	267	28	267
Material test	67	53	151.8	110.3	425.1	423.1
FBG and predictive model	71	52	162.3	105.7	424.9	422.8
Brakel-full restraint	22	1	16.0	/	419.5	417.2
Trost-full restraint	28	2	36.0	/	420.2	417.3
Brakel−64 % restraint	41	28	73.7	33.7	421.6	420.2
Trost−64 % restraint	45	29	86.6	36.4	422.1	420.3
Experiment	47	33	90	50	390.9 (no failure)	380.9

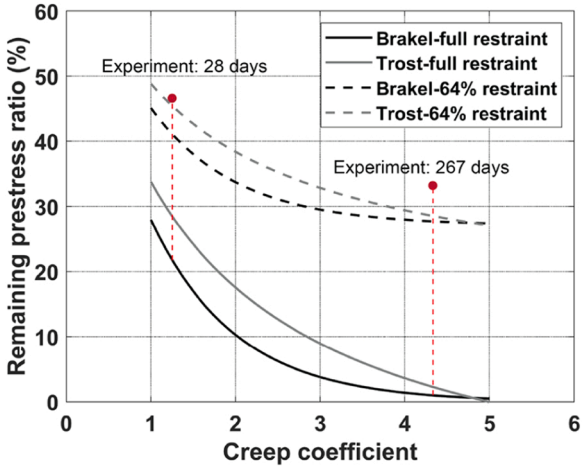

Fig. 20. Remaining prestress ratio considering restraint level.

coefficient, considering different levels of restraint, is shown in Fig. 20.

The residual prestress force is highly underestimated when a full restraint condition is assumed. However, when the restraint level is taken into account, the remaining prestress ratio at 28 days and 9 months after casting the topping concrete are much closer to the experimentally obtained values. Overall, the remaining prestressing force can be well estimated using the modified methods that consider the level of restraint, with the method proposed by Trost [40] providing a slightly better prediction than that of Brakel [39].

FBG sensor provides the possibility to measure the strain inside the girder, which can be used to predict prestress losses. However, the situation becomes more complex when deformations are restrained. Unlike imposed loads, restrained deformation (such as shrinkage and creep) does not exhibit a linear relationship between stresses and deformations - meaning that even when no deformation is measured, the structure can still experience stresses. Therefore, careful consideration should be given to sensor configuration and the analysis of strain measurement data when dealing with restrained deformations.

4.2. *Ultimate state*

The ultimate moment resistance in the cross-section at midspan is determined by an iterative calculation of the equilibrium of forces generated by the concrete, prestressing and reinforcement steel. Average values of material properties are applied and no safety factors are considered. The experimental and analytical maximum flexural load are listed in Table 4.

The predicted maximum loads are slightly higher than the experimental results for STF and LTF, by 8 % and 10 %, respectively. Note that although the horizontal debonding cracks were observed in the experiments, this phenomenon is not considered when estimating the maximum load. Besides, the analytical model for ultimate state prediction follows the assumption of flexural failure while anchorage failure occurred on LTF.

5. Conclusions

To investigate the time-dependent flexural behaviour of prestressed AAC girder with cast-in-situ AAC topping, a combined experimental and analytical study was conducted. Long-term mid-span deflection of the composite girders subjected to self-weight and sustained load under flexure was monitored. Flexural tests were carried out on three 7 m span specimens at 28 days and 9 months, and the material properties of the AAC mixtures were measured over time. With insights obtained from material and structural tests, analytical models were further applied to analyse the flexural behaviour of the composite girders, focusing on the

prediction of prestress losses. The following conclusions can be drawn:

- The splitting tensile strength of SCGC and elastic modulus of both AAC mixtures exposed to laboratory condition (20℃ and 55 % RH) decreased over time. Under the same condition, the compressive strength of SCGC stayed constant after 90 days. No reduction in mechanical properties was observed for samples that were moist cured. Furthermore, increased shrinkage and creep deformation were observed up to 1000 days and 400 days, respectively.
- The specimen subjected to sustained load (LTF_LS) reached a plateau in deflection, while unloaded specimen (LTF) showed a continuous increase in upward deflection, indicating pronounced ongoing creep effects up to the testing age.
- Compared with the specimen tested at 28 days (STF), the specimens tested at around 9 months showed significantly lower stiffness and lower cracking load. Around 44 % lower cracking load was observed in the specimen tested at 9 months (LTF) compared to 28 days (STF). The maximum crack width on the precast girders of specimens tested at 9 months reached the design criteria of 0.2 mm at lower load levels (160 kN for LTF and 180 kN for LTF_LS) compared to that of the specimen tested at 28 days (220 kN). The pronounced prestress loss seems to be a consequence of ongoing shrinkage and creep effects.
- Specimen LTF and LTF_LS exhibited different failure modes. In LTF, anchorage failure occurred at a lower load level than in STF, when the maximum stroke was reached. In contrast, LTF_LS displayed concrete crushing in the topping concrete, indicative of flexural failure.
- The bond behaviour between SCGC and prestressing strands plays a critical role in the time-dependent structural behaviour of the composite girders. Based on the crack pattern and reduced failure load (initiated by anchorage failure) in LTF compared to STF, it is anticipated that there is a bond decrease over time. The application of sustained load resulted in a lower stress level at the level of prestressing strands and therefore a reduced creep effect. Its beneficial effect on bond capacity is confirmed by the distinct failure mode of LTF_LS, which exhibited flexural failure at a higher load level than LTF.
- The analytical model based on material test data and strain (FBG) measurements, underestimated prestress loss and overestimated cracking load for both composite girders tested at 28 and 9 months. In this case, the interaction between the precast girder and topping concrete in terms of restrained shrinkage and creep effects was neglected. The influence of restrained deformation on composite girders has to be considered. The compressive stress at the strand level, and thus the additional prestress losses caused by restrained differential shrinkage between topping concrete and prestressed concrete, is low. The effects of restrained creep deformation of precast girder, however, contribute to significant additional prestress loss. By considering the restraint level, the predicted results of prestress losses show good agreement with the experimental results.

It is important to note that relying on structural tests at 28 days or on design guidelines for conventional concrete elements based on 28-day material properties is not suitable for verifying the structural resistance of AAC members, particularly for the AAC types used in this study. Significant time-dependent deformation was observed due to high shrinkage and creep in prestressed AAC, and this must be included in structural analysis along with appropriate long-term mechanical properties. Overall, it is crucial to investigate the long-term material and structural behaviour of AAC members in future studies.

There are a few limitations of the current study which should be considered in more detail in future. Firstly, the experiments were carried out within a period of 9 months and a longer time frame is suggested. Secondly, the debonding crack between precast girder and topping concrete observed in the experiments was not considered in the applied analytical models. Furthermore, although FBG sensors provided valuable measurements of time-dependent deformation inside the girder, the influence of restrained deformations cannot be captured by the current sensor configuration. Better design of the sensor layout and detailed analysis are recommended for future applications in the structural tests of composite girders.

CRediT authorship contribution statement

Qian Zhenxu: Writing – original draft, Investigation, Formal analysis, Conceptualization. **Zhang Shizhe:** Writing – review & editing, Investigation. **Ye Guang:** Writing – review & editing, Supervision, Funding acquisition. **Matthys Stijn:** Writing – review & editing. **Luković Mladena:** Writing – review & editing, Supervision, Conceptualization.

Declaration of Competing Interest

The authors declare that they have no known competing financial interests or personal relationships that could have appeared to influence the work reported in this paper.

Acknowledgements

This work was supported by the project “Toepassingsmogelijkheiden Geopolymerbeton in infrastructurele werken”, which was funded by Province Fryslan (project number CM2B17). The authors would like to express their gratitude for the obtained laboratory support.

Data availability

Data will be made available on request.

References

[1] P.K. Mehta, P. Monteiro, Concrete: Microstructure, Properties, and Materials, McGraw-Hill Publishing, 2006.
[2] R.M. Andrew, Global CO_2 emissions from cement production, Earth Syst. Sci. Data 10 (1) (2018) 195–217.
[3] I. Chang, M. Lee, G.-C. Cho, Global CO_2 emission-related geotechnical engineering hazards and the mission for sustainable geotechnical engineering, Energies 12 (13) (2019) 2567.
[4] K.-H. Yang, J.-K. Song, K.-I. Song, Assessment of CO_2 reduction of alkali-activated concrete, J. Clean. Prod. 39 (2013) 265–272.
[5] G. Habert, C. Ouellet-Plamondon, Recent update on the environmental impact of geopolymers, RILEM Tech. Lett. 1 (2016) 17–23.
[6] P. Zhang, K.X. Wang, Q.F. Li, J. Wang, Y.F. Ling, Fabrication and engineering properties of concretes based on geopolymers/alkali-activated binders - A review, J. Clean. Prod. 258 (2020).
[7] K.H. Mo, U.J. Alengaram, M.Z. Jumaat, Structural performance of reinforced geopolymer concrete members: a review, Constr. Build. Mater. 120 (2016) 251–264.
[8] M. Albitar, M.S.M. Ali, P. Visintin, Evaluation of tension-stiffening, crack spacing and crack width of geopolymer concretes, Constr. Build. Mater. 160 (2018) 408–414.
[9] D.M. Sumajouw, D. Hardjito, S. Wallah, B. Rangan, Behaviour and strength of reinforced fly ash-based geopolymer concrete beams, in: Proceedings of the Australian Structural Engineering Conference 2005, Engineers Australia Sydney, NSW, 2005, 453-459.
[10] A. Shah, C. Shah, Comparison of load-displacement relationship and crack development mechanism in reinforced geopolymer concrete beams with that of regular reinforced concrete beams, in: Proceedings of the International Conference on Advances i n Construction Materials and Systems, Chennai (2017).
[11] S. Prinsse, D.A. Hordijk, G. Ye, P. Lagendijk, M. Lukovic, Time-dependent material properties and reinforced beams behavior of two alkali-activated types of concrete, Struct. Concr. 21 (2) (2020) 642–658.
[12] J.R. Yost, A. Radlinska, S. Ernst, M. Salera, N.J. Martignetti, Structural behavior of alkali activated fly ash concrete. Part 2: structural testing and experimental findings, Mater. Struct. 46 (3) (2013) 449–462.
[13] Z. Qian, E.O. Lantsoght, M. Lukovic, A critical review on structural behavior of alkali-activated concrete beams, in: Proceedings of the Fourteenth Fib International Ph.D. Symposium in Civil Engineering, Rome (2022) 273–280.
[14] C. Luan, Q. Wang, F. Yang, K. Zhang, N. Utashev, J. Dai, X. Shi, Practical prediction models of tensile strength and reinforcement-concrete bond strength of low-calcium fly ash geopolymer concrete, Polymers 13 (6) (2021) 875.

[15] H.H. Liu, Z.A. Lu, Z.Q. Peng, Test research on prestressed beam of inorganic polymer concrete, Mater. Struct. 48 (6) (2015) 1919–1930.
[16] T. Sonal, D. Urmil, B. Darshan, Behaviour of ambient cured prestressed and non-prestressed geopolymer concrete beams, Case Stud. Constr. Mater. 16 (2022).
[17] F. Collins, J.G. Sanjayan, Microcracking and strength development of alkali activated slag concrete, Cem. Concr. Comp. 23 (4-5) (2001) 345–352.
[18] H.J. Bezemer, N. Awasthy, M. Lukovic, Multiscale analysis of long-term mechanical and durability behaviour of two alkali-activated slag-based types of concrete, Constr. Build. Mater. 407 (2023).
[19] F. Collins, J.G. Sanjayan, Effect of pore size distribution on drying shrinking of alkali-activated slag concrete, Cem. Concr. Res. 30 (9) (2000) 1401–1406.
[20] F.G. Collins, J.G. Sanjayan, Workability and mechanical properties of alkali activated slag concrete, Cem. Concr. Res. 29 (3) (1999) 455–458.
[21] Z.M. Li, B. Delsaute, T.S. Lu, A. Kostiuchenko, S. Staquet, G. Ye, A comparative study on the mechanical properties, autogenous shrinkage and cracking proneness of alkali-activated concrete and ordinary Portland cement concrete, Constr. Build. Mater. 292 (2021).
[22] A. Kostiuchenko, Creep of Alkali-activated Fly Ash and Slag Concrete: Unveiling Multiscale Dynamics, Delft University of Technology, Delft, 2024.
[23] C.H. Un, J.G. Sanjayan, R. San Nicolas, J.S.J. van Deventer, Predictions of long-term deflection of geopolymer concrete beams, Constr. Build. Mater. 94 (2015) 10–19.
[24] S. Zhang, G. Ye, M. Lukovic, H. Hendrik, A. Scharringa, Geopolymeerbeton voor infrastructurele toepassingen (1): Ontwikkeling van zelfverdichtende mengsels, Cem. Vakbl. voor De. Beton 2022 (7) (2022) 42–50.
[25] S.J. Lokhorst, Deformational Behaviour of Concrete Influenced by Hydration Related Changes of the Microstructure (1999).
[26] B. Espion, P. Halleux, Long term behavior of prestressed and partially prestressed concrete beams: experimental and numerical results, Spec. Publ. 129 (1991) 19–38.
[27] J. Purkiss, P. Blagojević, Comparison between the short and long term behaviour of fibre reinforced and unreinforced concrete beams, Compos. Struct. 25 (1-4) (1993) 45–49.
[28] X. Liu, W. Yu, Y. Huang, G. Yang, W. You, L. Gao, J. Song, Long-term behaviour of recycled aggregate concrete beams prestressed with carbon fibre-reinforced polymer (CFRP) tendons, Case Stud. Constr. Mater. 18 (2023) e01785.
[29] NEN-EN 1991-2+C1/NB, Eurocode 1: Belastingen op constructies – Deel 2: Verkeersbelasting op bruggen, Nederlands Normalisatie Instituut, 2019.
[30] N. Awasthy, E. Schlangen, D. Hordijk, B. Savija, M. Lukovic, The role of eigen-stresses on apparent strength and stiffness of normal, high strength, and ultra-high performance fibre reinforced concrete, Dev. Built Environ. 16 (2023).
[31] Z.M. Li, S.Z. Zhang, X.H. Liang, G. Ye, Cracking potential of alkali-activated slag and fly ash concrete subjected to restrained autogenous shrinkage, Cem. Concr. Compos. 114 (2020).
[32] M. Nedeljkovic, B. Savija, Y.B. Zuo, M. Lukovic, G. Ye, Effect of natural carbonation on the pore structure and elastic modulus of the alkali-activated fly ash and slag pastes, Constr. Build. Mater. 161 (2018) 687–704.
[33] S.A. Bernal, J.L. Provis, R.M. de Gutiérrez, J.S.J. van Deventer, Accelerated carbonation testing of alkali-activated slag/metakaolin blended concretes: effect of exposure conditions, Mater. Struct. 48 (3) (2015) 653–669.
[34] EN 1992-1-1 Eurocode 2, Design of Concrete Structures-Part 1-1: General Rules and Rules for Buildings, European Committee, 2005.
[35] B. Svensvik, Zum Verformungsverhalten gerissener Stahlbetonbalken unter Einschluss der Mitwirkung des Betons auf Zug in Abhängigkeit von Last und Zeit, Technische Universität Braunschweig, Braunschweig, 1981.
[36] R.W. Barnes, J.W. Grove, N.H. Burns, Experimental assessment of factors affecting transfer length, Acids Struct. J. 100 (6) (2003) 740–748.
[37] S. Zhang, Cheng, H., Yang, Y., Monitoring of Prestressed Geopolymer Girders using Smart Aggregates and Fibre Optic Sensors, 2022.
[38] Z.P. Bažant, M. Jirásek, Creep and Hygrothermal Effects in Concrete Structures, Springer, 2018.
[39] J. Brakel, Betonnen bruggen, Technische Hogeschool.
[40] H. Trost, B. Mainz, H. Wolff, Zur Berechnung von Spannbetontragwerken im Gebrauchszustand unter Berücksichtigung des zeitabhängigen Betonverhaltens, Beton-U Stahlbetonbau 66 (9 & 10) (1971).